Liu Yan (Orcid ID: 0000-0003-3197-9349)
Reible Danny (Orcid ID: 0000-0002-3188-9709)
Fang Hongwei (Orcid ID: 0000-0002-5621-6279)

Role of bioroughness, bioirrigation and turbulence on oxygen dynamics at the Sediment-Water Interface

Y. Liu[1], D. Reible[1], F. Hussain[2], and H. Fang[3]

[1]Department of Civil & Environmental Engineering, Texas Tech University, Lubbock, TX 79409, USA

[2]Department of Mechanical Engineering, Texas Tech University, Lubbock, TX 79409, USA

[3]Department of Hydraulic Engineering, Tsinghua University, Beijing, 100084, China

Corresponding author: Danny Reible(danny.reible@ttu.edu)

Key Points:

- This study quantifies the effects of organism mounds and burrows on oxygen transport over the sediment-water interface (SWI). Organism mounds and burrows substantially alter the surface roughness (bioroughness) and flow and oxygen transport over the SWI and the coupling between surface flow and subsurface flow.
- The enhanced O_2 transport scales with roughness height and roughness Reynolds number, and is described well by the relationship of O'Connor and Harvey (2008) ($D_e/D'_m = 0.005\, Re_*\, P\, e^{1.2}$) when flow is effectively 2 D. We propose a new scale (burrow number, Bu), where Bu = [burrow density]$^{1/2}$[burrow height], and find this conclusion to hold for Bu<0.05.
- The O_2 transport increases by as much as a factor of 4 under mound-induced three-dimensional flow when there are substantial interactions between the flow over adjacent mounds, i.e. for Bu>>0.1.
- Bioirrigation also enhances oxygen transport and generates asymmetric distributions of O_2 around burrows, although the influence of bioirrigation becomes negligible at high roughness Reynolds numbers.

This article has been accepted for publication and undergone full peer review but has not been through the copyediting, typesetting, pagination and proofreading process which may lead to differences between this version and the Version of Record. Please cite this article as doi: 10.1029/2019WR025098

Abstract

Models that have been developed to quantify the oxygen flux at the sediment-water interface (SWI) generally do not explicitly consider the influence of bioroughness (mounds and burrows) and bioirrigation. We performed a numerical study of the influence of overlying water velocity, bioroughness, and bioirrigation on the oxygen flux across the sediment-water interface. We found that compared with a flat bed, bioroughness significantly increases O_2 transport at the SWI as a result of enhanced turbulence and pressure differences across the roughness. Bioirrigation can also enhance O_2 transport across the SWI by a factor of up to 10 when the roughness Reynolds number (Re_*) is low, but the influence of bioirrigation decreases with increasing Re_*. Burrows increase O_2 penetration depth, and bioirrigation causes asymmetric distributions of O_2 along burrows. Despite the complexity of O_2 distribution in sediments, the net exchange across the SWI can be described by the relationship of O'Connor and Harvey (2008)$\left(\frac{D_e/D_m}{Re_* Pe^{1.2}} = a = 0.0005\right)$ when the shape is 2 dimensional or when the burrow density is low. When the burrow density is large, flow is 3 dimensional and flow interactions between burrows become important. Under these conditions the net exchange across the SWI increases by up to a factor of 4. A burrow number is introduced, Bu = [burrow density]$^{1/2}$[burrow height], to correct the coefficient in O'Connor and Harvey's relationship, i.e. a=0.005 for Bu<0.05 and a=0.02 for Bu>>0.1.

1 Introduction

Oxygen flux across the Sediment-Water Interface (SWI) drives the biogeochemistry in surficial sediments. The metabolic energy available to an organism for each mole of carbon utilized during decomposition of organic matter depends in part on the electron acceptor involved and progressively decreases in the order O_2>NO_3^->MnO_2>FeOOH>SO_4^{2-}>CO_2 (McCall & Tevesz, 1982). This controls nutrient cycling in sediments as well as the behavior and effects of redox sensitive contaminants such as metals. Enhanced O_2 flux at the SWI can lead to the oxidation of acid-volatile sulfide (Kelderman & Osman, 2007; Teuchies et al., 2011), resulting in dissolution of metals and enhanced flux of metals to the overlying surface (Teuchies et al., 2011). The nitrate produced by nitrification in the oxic zone will stimulate denitrification when the sediment in the same location changes to anoxic condition, promoting release of N_2 (Huettel et al., 2014). The sediment oxygen demand will reduce oxygen levels in the overlying water, stressing fish and other species (Hölker et al., 2015).

It is commonly observed that animal burrowing and bioturbation can influence the O_2 flux (Frogner-Kockum et al., 2016; Hölker et al., 2015; Volkenborn et al., 2012; Ziebis et al., 1996b). Burrowing animals such as ghost shrimp (Volkenborn et al., 2012) and polychaete worms (Xie et al., 2018) introduce several features that can influence local O_2 transport. The removal of sediment for the organism burrow will lead to dune-like structures at the mouth of the burrow as well as increase voids and overall permeability of the sediment. Flume studies have demonstrated that hydrodynamics is a crucial driver of benthic O_2 dynamics in permeable sediments (Forster et al., 1996; Reimers et al., 2004) and in situ (Berg et al., 2013; Cook et al., 2007). Structures as small as 700 μm exposed to water speeds as low as 3 cm/s have been observed to produce an in-bed advective flow (Huettel & Gust, 1992). Tracks produced on the sediment surface by foraging animals, mounds of fecal matter, protruding siphons of clams, and shell fragments scattered on the sediment surface, all can lead to enhanced pore-water exchange. Realistic abundances of such structures enhance interfacial solute flux in coastal sands by factors of up to 10 (Huettel & Gust, 1992). O'Connor and Harvey (referenced hereafter as OH) correlated measurements from a range of two dimenional flume and field data on isolated burrows, and their results show that the dimensionless effective diffusion coefficient D_e for net oxygen transport can be expressed as a function of Reynolds number and Peclet number as $\frac{De}{D'm} = 5 \times 10^{-4} Re_* Pe_k^{6/5}$, where Re_* is defined as $Re_* = \frac{u_* k_s}{\upsilon}$ and $Pe_k = \frac{u_* \sqrt{k}}{D'_m}$. u_* is the friction velocity, k_s is the roughness height (k_s =mound height), D'_m is the effective molecular diffusion coefficient for O_2 in the sediment under static conditions, and k is the sediment permeability. The *OH* relationship describes only the net O_2 flux across the SWI but does not describe how O_2 is distributed. Several researchers have reported asymmetric O_2 distributions in the presence of bedforms for permeable sand beds (Cardenas & Wilson, 2007; Packman et al., 2004; Savant et al., 1987).

In addition, organisms can pump water through these burrows during the process of feeding or respiration, which generates pressure gradients in the burrows and at the SWI (Ahmerkamp et al., 2017; Brand et al., 2013). The pressure gradient can enhance advective pore water bioirrigation in permeable sandy sediments (Kristensen et al., 2012). O_2 flux caused by bioirrigation has been estimated to account for 14% of the total O_2 flux around the world (Huettel et al., 2014; Santos et al., 2012). To quantify oxygen flux induced by bioirrigation, several methods have been used, including benthic flux chambers (Webb & Eyre, 2004), resazurin tracer (Baranov et al., 2016b), lifetime-based laser induced fluorescence (Murphy & Reidenbach, 2016) and an eddy covariance method (Attard et al., 2016). These methods confirm that sediment respiration is enhanced by a factor of 2-3 by bioirrigation (Baranov et

al., 2016b; Pascal et al., 2016), and these methods have been successfully applied to investigate the interaction of temperature fluctuations and bioirrigation (Baranov et al., 2016a) and temporal and spatial variations in O_2 dynamics during bioirrigation (Murniati et al., 2017). These approaches, with the exception of the eddy covariance approach, exclude the effects of the overlying water flow. An experiment investigating the effects of interaction of bioturbation and overlying water flow on Cu efflux shows that the interaction of hydrodynamics and bioturbation can enhance Cu efflux relative to the effects of flow alone as well as effects of bioturbation alone (Xie et al., 2018). This is likely the result of sulfide oxidation (Hong et al., 2011) due to increased O_2 flux at the SWI.

Here we perform numerical simulations to study the impact of bioroughness and bioirrigation on the oxygen distribution in sediments and O_2 exchange at the SWI. By varying the overlying water velocity U_{water}, the ratio of water velocity to burrow bioirrigation velocity, and the areal density of burrows, we examine the effects of flow, bioirrigation, bioroughness and 3 dimensional flow interactions between burrows. Specific questions we address include: (1) how does bioroughness influence the O_2 dynamics at the SWI with increasing overlying water velocity, U_{water}? (2) how does bioirrigation interact with bioroughness and influence the O_2 flux? And (3) what is the effect of 3 dimensional flow interactions between burrows as their density increases? The results of the numerical simulations are compared to available experimental data and empirical models of bulk O_2 transport generated from those experiments.

2 Materials and Methods

2.1 Governing Equations

In this study the method of large-eddy simulation (LES), using the code Hydro3D, an eddy-resolving numerical method, is used for the overlying water. Hydro3D has been validated and applied to several flows of similar complexity to the one reported here (Fang et al., 2017; Liu et al., 2017; Ouro et al., 2017; Ouro & Stoesser, 2017). The code is based on finite differences on a staggered Cartesian grid and solves the filtered Navier-Stokes equations for incompressible, unsteady and viscous flow:

$$\frac{\partial u_i}{\partial x_i} = 0 \tag{1}$$

$$\frac{\partial u_i}{\partial t} + \frac{\partial u_i u_j}{\partial x_j} = -\frac{1}{\rho}\frac{\partial p}{\partial x_i} + \frac{\partial \left(2\nu S_{ij}\right)}{\partial x_j} - \frac{\partial \tau_{ij}}{\partial x_j} \tag{2}$$

where u_i or u_j is the resolved velocity vector (i or j = 1, 2, and 3 represent x-, y- and z-axis directions, respectively); and similarly x_i represents the spatial vectors in the three directions; ρ is water density; p is the resolved pressure above hydrostatic pressure; υ = kinematic viscosity; and S_{ij} is the strain-rate tensor. The sub-grid scale (SGS) stress is defined as $\tau_{ij} = -2\nu_t S_{ij}$ and in this study the wall-adapting local eddy viscosity (WALE) model proposed by Nicoud and Ducros (Nicoud & Ducros, 1999) is used to compute the SGS stress. The turbulent sub-grid scale eddy viscosity, ν_t, is calculated in this model.

The convection and diffusion terms in the Navier-Stokes equations are approximated by 4th-order accurate central differences. An explicit 3-step Runge-Kutta scheme is used to integrate the equations in time, providing 2nd-order accuracy. A fractional step method is employed; convection and diffusion terms are solved explicitly first in a predictor step which is then followed by a corrector step during which the pressure and divergence-free-velocity fields are obtained through a Poisson equation. The latter is solved iteratively through a multi-grid procedure. More details of the code are reported in Cevheri & Stoesser (2018). Both 2 dimensional and 3 dimensional simulations are conducted. Most experimental data has been

collected in 2 dimensional flumes or with isolated organism burrows; so the model is initially validated in 2 dimensions and then used to predict 3 dimensional behavior at different burrow densities.

The flow is modeled explicitly in sediment voids created by the burrows but the flow in the surrounding consolidated sediment is assumed to be governed by continuity and Darcy equations:

$$\frac{\partial u_i}{\partial x_i} = 0 \tag{3}$$

$$u_i = -\frac{k}{\mu}\frac{\partial p}{\partial x_i} \tag{4}$$

where k is the permeability of the porous medium, μ is the dynamic viscosity of water (0.001 Pa·s). Combining equation (3) and (4), we obtain the Poisson equation (5) and we use the same multi-grid method as used for free fluid motion to solve equation (5).

$$\frac{\partial}{x_i}\left(\frac{\partial p}{\partial x_i}\right) = 0 \tag{5}$$

The solute transport is calculated using the advection-diffusion equation:

$$\frac{\partial c}{\partial t} + u_j\frac{\partial c}{\partial x_j} - D'_m\frac{\partial^2 c}{\partial x_j\,\partial x_j} = R \tag{6}$$

where c is the solute concentration, D'_m is the effective diffusion coefficient in sediments and R is the reaction rate, e.g. oxygen consumption rate. The effective diffusion coefficient of dissolved oxygen in the sediment pore system (D'_m) is a function of sediment porosity ($\emptyset$) and sediment tortuosity (θ) (Boudreau, 1997):

$$D'_m = \frac{\emptyset}{\theta^2}D_m \tag{7}$$

Based on an empirical relationship between volume averaged tortuosity and porosity, the diffusion coefficient can be expressed as a function of the sediment porosity (Boudreau & Jorgensen, 2001):

$$D'_m = \emptyset^3 D_m \; for \; \emptyset > 0.7 \tag{8a}$$

$$D'_m = \emptyset^2 D_m \; for \; \emptyset < 0.7 \tag{8b}$$

we used a D_m value of $1.97*10^{-9}$ m^2/s, which corresponds to the diffusion coefficient of oxygen at 20C° for all model calculations (Maerki et al., 2004). In the sediment, R is described using first-order kinetics:

$$R = -k_r c \tag{9}$$

for reactive solutes, e.g. oxygen. In the burrow and the overlying water, we assumed that O_2 consumption is negligible. For permeable marine sediments, the bulk sediment respiration rate summarized by Huettel et al. (2014) from 15 literature sources is in the range of 6 to 283 *mmol*/m^{-2}/d^{-1}. Considering an O_2 penetration depth of 4 mm for flat permeable sediments (See Figure 4) and average O_2 concentration in the sediment approximately half of the O_2 concentration in the overlying water (assumed saturated), this corresponds to a reaction rate constant f 0.48 h^{-1} to 22.67 h^{-1}. This is also similar to the range of O_2 consumption rates estimated for freshwater lake sediments by Brand et al. (2013) (k_r=1 h^{-1} to 40 h^{-1}). Therefore, we chose a representative reaction rate constant of k_r=10 h^{-1} for both lake sediments and permeable marine sediments and use a sensitivity analysis to examine both higher and lower reaction rates.

2.2 Numerical Setup and Boundary Conditions

Several kinds of benthic fauna are observed to dig burrows in sediments, such as thalassinid shrimp, razor clams, chironomid larvae and polychaete (marine) and olicogchaete (freshwater) worms (Kristensen et al., 2012). Polychaete worms are widely observed in muddy and sandy coastal areas (Renz & Forster, 2014; Volkenborn et al., 2007); they often construct

U- and J-shaped burrows, 6 to 35 cm deep, 2 mm mean diameter (Quintana et al., 2011; Renz & Forster, 2013). Thalassinid shrimp construct U-shaped burrows in muddy sand and sand, 10 cm to 30 cm deep, 1~2 cm diameter (Volkenborn et al., 2012; Ziebis et al., 1996a). The typical burrows described by Ziebis et al. (1996a) of *Callianassa truncata (Decapoda: Thalassinidea),* are employed in this work because of the availability of velocity data with which to compare the model. The implications for other burrow geometries will be discussed.

Ziebis et al. (1996a) investigated the burrow geometry of *C. truncata* from field observations. They reported the dimensions for a *C. truncata* burrow, with burrow diameter approximately 2 cm, burrow depth 5 to 10 cm, mound height 1 to 9 cm, and burrow densities of up to 120 per m^2. They subsequently carried out flume experiments (200 cm long, 30 cm wide and 12 cm deep) studying the influence of the burrow mounds (1 cm in height) on flow velocity and O_2 transport (Ziebis et al., 1996b). In their flume experiments, they chose a flow velocity of 6.5 cm/s at 5 cm above sediment surface to represent natural tidal flow (2 cm/s to 16 cm/s at 5 cm above sediment surface in field observation). Ten velocity profiles were measured starting 5 cm upstream of the *C. truncata* mound and continuing in the direction of flow (See Figure 1). Starting at a height of 20 mm above the sediment surface the flow velocity was measured at 1 mm intervals toward the sediment. For each step the data was recorded for 30 s. We set up three sets of numerical simulations in an equivalent system, one for flow over flat rough sand beds (Flat), one for flow over abandoned burrows (Bioroughness only) and the third for flow over burrows with organism bioirrigation (Bioirrgiation and bioroughness). The domain for all simulations is 75 cm in length, 30 cm in width, 5 cm of water depth and 10 cm of sediment depth (Fig. 1). The SWI is represented by z=0 cm (red surface in Figure 1).

In our simulations with burrows, we keep the burrow dimensions (mound height, mound diameter, burrow diameter), flow hydrodynamics (flow velocity, water depth) and sediment properties (medium grain size, permeability, porosity) to be consistent with the experiments of Ziebis et al. (1996a,b) as shown in Table 1. We use a half-circular ring to represent the organism burrow with an inner radius of 3 cm and an outer radius of 5 cm. Thus, the burrow has a horizontal length of 10 cm, a depth of 5 cm, an inside diameter of 2 cm. We assume an average flow of 60 mL/min per burrow as an average bioirrigation rate. The bioirrigation flow rate of this specie is unknown, but the selected value is similar to that reported for a mud shrimp, *Upogebia major*, 50 ml/min per burrow (Koike & Mukai, 1983). Given the dimensions of the burrow this corresponds to U_{bio}=2 cm/s in the burrow.

We vary the overlying water velocity from 2 cm/s to 16 cm/s (Table 1), a range of values that encompasses the region where such organisms and burrows have been reported by Ziebis et al. (1996b). The Reynolds number based on water depth H_{water}, overlying water velocity U_{water} and water kinematic viscosity, υ, varies from 1000 to 8000. The bioirrigation is simulated by applying an axial force at the lowest level of the burrow in a manner similar to Brand et al. (2013). The resulting parabolic flow is maintained at an average of 2 cm/s over the burrow cross-section. The sediment permeability, $k=5.1*10^{-11}$ m^2, sediment diameter, d_s=0.35 mm and porosity, $\emptyset$=0.4, are chosen to be the same as those in the Bay of Campese, Isola del Giglio, Italy (42°20' N, 10°52' E) where the shrimp mounds and burrows are observed at a density of 120 per m^2. We varied the permeability of the sediments over the range suggested by Huettel et al. (2014) of 10^{-9} to 10^{-12} m^2 to evaluate sensitivity to this parameter.

We compared the pressure distribution at the SWI and velocity profiles in the overlying water on three different meshes; a coarse mesh of 360×144×72, a medium mesh of 720×288×144, and a fine mesh of 1440×576×288. The highest grid resolution in wall units defined by the friction velocity and kinematic viscosity $\Delta^+ = {\Delta \cdot u_*}/{\upsilon}$, is obtained on flat rough

beds when U_{water}=2 cm/s ($\Delta x^+ = \Delta y^+ = \Delta z^+ \approx 0.8$), and the lowest grid resolution in wall units is obtained in case of mound and burrow without bioirrigation when U_{water}=16 cm/s ($\Delta x^+ = \Delta y^+ = \Delta z^+ \approx 18$).

The boundary conditions for the flow and O_2 in the overlying flow is set as periodic in the streamwise (x direction) and spanwise directions (y direction). For the streamwise direction, a spatial-uniform body force is applied for the whole domain to drive the flow. The body force is adjusted every time step according to the cross-averaged velocity at the domain outlet to achieve the target averaged velocity, U_{water}. The water surface is modeled as a free slip condition and saturated with O_2. We assume that the flow across the sediment-water interface is negligible compared to the overlying water flow so that a no-slip condition is applied to the sediment by the direct forcing immersed boundary method proposed by Uhlmann (2005). Continuity of O_2 concentration and flux is assumed across the SWI interface.

The pressure distribution at the SWI calculated from LES is used to drive the Darcy flow in the sediment. The streamwise and spanwise direction is also set to be periodic for flow and O_2 in the sediment. A no-slip condition is applied for the flow at the bottom of the computational domain, where the O_2 concentration is set to zero (although the sediment layer is deep enough that the reactive O_2 approaches 0 before reaching this boundary).

3 Results

3.1 Model Validation

As noted previously, model validation is conducted in 2D since most experimental data is available from 2D flumes or isolated burrows that are not influenced by adjacent burrows. Figure 2 shows the time-averaged streamwise velocity profiles at cross section A to J (in Fig. 1) for three different meshes compared with experimental data from Ziebis et al. (1996b). Our simulated results agree reasonably well with the measured data except some discrepancies in the near bed region. The experimental velocity profile near the SWI is sensitive to surface conditions (particularly at sections A, B, C and D) and there is substantial scatter in the data at some cross sections (D, E, F) in the region H<0.5 cm, which may be caused by the short duration of averaging in the measurements (30s). Despite these discrepancies, our results successfully captured the main features of the flow over a single mound, including flow acceleration upstream of the mound and wake zone downstream of the mound. The differences between the medium and fine mesh are negligible. Therefore, all subsequent calculations are carried out on the medium mesh of 720×288×144, in the x-, y- and z- directions. As we are using the pressure distribution at the SWI from LES as the boundary for calculating Darcy flow in the sediment, we also plot the pressure distribution at the SWI for the three meshes in Figure 3. The results of velocity and pressure both suggest the medium mesh to be sufficient in simulating flow and O_2 exchange at SWI.

3.2 Influence of Bioroughness

Figure 4 plots the time-averaged O_2 concentration distribution in the sediment for U_{water}=10 cm/s, over a flat sand bed compared to the bed with bioroughness. For the flat sand bed, O_2 penetrates uniformly into the sediments. We compared the oxygen distribution in the sediments with the measured profiles from Ziebis et al. (1996b). The simulated profile agrees well with the data.

The appearance of bioroughness alters the distribution of O_2 in the sediment, increasing the penetration depth (defined as the depth below the SWI where O_2 concentration is C/C_w=0.1) upstream of the mound (x<-5 cm) and further downstream of the mound (x>1 cm). We also compare the O_2 profiles at three locations (x=-12 cm, -7 cm and -6 cm) with the data reported from Ziebis et al. (1996b). Our model simulates the O_2 profile at x=-12 cm (A) well, where O_2 penetration is dominant by diffusion. The model slightly underestimates the O_2 penetration depth and O_2 concentration in the sediment for x=-7 cm (B) and x=-6 cm (C). The underestimation is probably due to the difference of bed morphology between the experiments and our simulations. There is small roughness of height 2-3 mm nonuniformly distributed upstream of the mound in the experiments (Ziebis et al., 1996b), while we do not simulate the small roughness. Despite the underestimation, our model is able to capture the general influence of the organism mound on O_2 distribution in the sediment.

3.2 Influence of Bioirrigation

Figure 5 plots the time-averaged pressure and velocity contours with streamlines for simulations U_{water}=2 cm/s with and without bioirrigation. A high pressure zone on the upstream side of the mound and a low pressure zone on the downstream side are observed without bioirrigation (Fig 5(a)). Overlying water is pumped into the sediment due to the elevated upstream pressures and out of the low pressure zone. The highest Darcy velocity is observed underneath the upstream side of mound (Fig. 5(c)).

With bioirrigation from upstream to downstream through the burrow at a velocity U_{bio}=2 cm/s, the pressure distribution is significantly altered and pressure gradients and advective flows in the sediment increase in magnitude. The highest pressure zone is observed where the bioirrigation exits the burrow and lowest pressure (highest negative pressure) is on the upstream inlet side of the burrow (Fig. 5(b)). Note that in Fig. 5(d) the thick lines starting at about z=2.5 cm separate the mean stream flow from that which enters the burrow and the bed. The pressure above the bed at x=1 cm is high because of the streamline curvature and pressure is low at x=-4.5 cm due to the mound. The separation downstream of the burrow in Fig. 5(d) is due to the jet-like bioirrigation flow exiting from the burrow.

The O_2 distribution in sediments around burrows is also influenced by bioroughness and bioirrigation (Figure 6). Without bioirrigation, the oxygen concentration is distributed quite uniformly along the sediment-water interface as well as the burrow wall, except a slight increase in O_2 penetration depth upstream of the mound from x=-8 cm to x=-5 cm (Fig. 6(a)). With bioirrigation, the O_2 penetration depth is significantly increased both upstream of the mound from x=-10 cm to x=-5 cm (point 1) and downstream, from x=-3 cm to x=3 cm (point 2) (Fig. 6(b)). The O_2 concentration is distributed asymmetrically along the burrow bottom wall with more O_2 penetrating into the sediment from x=0 cm to x=5 cm (point 3) compared to that from x=-5 cm to x=0 cm. Not surprisingly, O_2 penetration depth increases where there is inflow (from water to sediment) while it decreases in outflow regions. There is a substantial increase in oxygen penetration into the sediment above the burrow. Note that despite the increase in overall sediment oxygen demand with bioirrigation, the water remains saturated with O_2 at the SWI, i.e. mixing in the overlying water remains sufficiently fast that O_2 transport remains controlled by sediment-side processes.

3.3 Influence of overlying flow velocity

The influence of overlying flow velocity is investigated by varying U_{water} from 2 cm/s to 16 cm/s at 2 cm/s intervals. For the Flat case, increasing U_{water} results in an increase of O_2 penetration depth (59% increase as U_{water} goes from 2 cm/s to 16 cm/s; Figure S1 in supporting information). This is due to the enhanced turbulence-induced pressure fluctuation near the SWI.

In the Bioroughness case, increases in U_{water} gives rise to approximately quadratic increases in pressure gradients (Fig. 7(a)). The convective and O_2 fluxes are also increased, due not only to the increased mean pressure gradients on the SWI but fluctuations in pressure at the surface due to the increased turbulence. At 16 cm/s, approximately 23% of the flux across the SWI is due to the turbulent fluctuations (Figure S6 in supporting information). The increased flux through the SWI results in substantial increases in O_2 penetration depths. (Fig. 7(b)). Between the mound and burrow outlet (-3 cm<x<3 cm), almost all the sediment above the burrow top wall maintains oxic conditions.

At higher velocities in the bioirrigation cases, the basic features of bioirrigation on pressures and O_2 penetration remain but are increasingly dominated by the effects of bioroughness. As shown in Fig. 8, the asymmetry of the bioirrigation remains but the overall magnitude of pressure gradients and the O_2 penetration is largely controlled by the bioroughness at highest simulated velocity.

3.4 Area-averaged effective diffusion coefficient

Both bioroughness and bioirrigation significantly influence the spatial variations in pressure and O_2 penetration but the net impact on water and sediment quality is controlled by areal-averaged O_2 flux. We compared average O_2 flux to the relationship proposed by OH. The effective diffusion coefficient D_e is calculated according to the Fick's first law at the SWI:

$$J = -D_e \frac{dC}{dz}|_{z=0} \tag{10}$$

Figure 9 plots the effective diffusion coefficient calculated from our 2 dimensional LES simulations and from several flume experiments along with the empirical formula proposed by OH. The effective diffusion coefficients calculated from our LES simulations without bioirrigation and LES simulation over flat sand beds at high U_{water} are in the range of measured data of flow over glass bead beds (Lai et al., 1994; Richardson & Parr, 1988), over triangles (Elliott & Brooks, 1997) and over ripples (Packman et al., 2000). We compare in Table 2 the hydraulic parameters used in the current study with the experiments. All the key parameters fall in the range of the experimental data, which may explain the close agreement between our bioroughness case with the formula. For flow over flat beds when $Re_*Pe_k^{1.2}<2*10^3$, the effective diffusion coefficient equals to the molecular diffusion coefficient in sediments. All simulated results for cases of flat rough bed and bioroughness agree well with OH's formula. This also suggests that roughness largely controls net O_2 transport and whether the roughness results from mounds at burrow mouths or other forms of roughness matters little.

With bioirrigation, the effective diffusion coefficient is significantly higher than all the measured results when $Re_*Pe_k^{1.2}<10^5$ and cannot be predicted by empirical formulas for flux over bedforms (OH). For the lowest water velocity flow, *De/D'm* increases approximately 10 times due to the bioirrigation behavior of organisms. For $RePe_k^{1.2}>10^5$, however, the bioirrigation induced flux at SWI (z=0) becomes insignificant compared with the bioroughness induced flux, and the OH formula is again valid.

3.5 Sensitivity of Results to O_2 Consumption Rate and Bed Permeability

In our simulations, we have several input parameters which could vary greatly in nature, including the oxygen reaction rate and sediment permeability. Simulations were conducted varying the reaction coefficient rate from 4 h^{-1} to 40 h^{-1}, with a permeability of $k=5.1*10^{-11}$ m^2 and $U_{water}=16$ cm/s. With a constant reaction rate of $k_r=10$ h^{-1}, we also varied the permeability from 10^{-12} m^2 to 10^{-9} m^2, with $U_{water}=16$ cm/s. The O_2 penetration depth changes as a result of these changes in conditions (See SI) with greater O_2 penetration for lower reaction rates and higher permeability due to the expected changes in advective transport of O_2.

The effects of these changes on the average O_2 transport rate or sediment oxygen demand, however, does not differ substantially from the OH formula as shown in Figure 10. Note that changes in permeability, in particular, lead to orders of magnitude change in *De/D'm*, but the magnitude of $Re_*Pe_k^{1.2}$ is also altered and the effect of permeability is to move values approximately up and down the OH formula. There are modest deviations from the formula, typically much less than a factor of 2, and these variations under different conditions may explain some of the scatter of the data in Figure 9. The results suggest that $Re_*Pe_k^{1.2}$ remains the dominant parameter influencing *De/D'm* but other factors may also cause some variations.

3.6 Comparison of 2D and 3D simulations

A major limitation of 2D modeling is that it cannot describe flow interactions between burrows or O_2 transport in the spanwise direction. To investigate the transverse O_2 transport, we also simulated 3D burrows with $U_{water}=16$ cm/s. We increased the burrow individual density from 4 ind./m^2 (individuals/m^2) to 120 ind./m^2. Flow simulations show that the pressure distribution between mounds alters the Darcy flow and O_2 in the sediment.

The O_2 distributions in the sediment for 4 ind./m^2 and 120 ind./m^2 are shown in Figure 11. Figures 11(a) and (d) show the time-averaged O_2 distribution in the sediment along the centerline of the 3D burrow for 4 ind./m^2 and 120 ind./m^2. The distribution of O_2 for 4 ind./m^2 in the sediment looks similar to that around a 2D burrow (Fig. 7d), except it exhibits a lower penetration depth at the SWI due to spanwise transport. Figures 11(b) and (e) plot the O_2 distribution in the sediment at y=13 cm for 4 ind./m^2 and 120 ind./m^2, respectively, which is 1 cm outside the burrow wall in the spanwise direction. The injection of O_2 upstream is significant for 120 ind./m^2, while for 4 ind./m^2 the influence of bioroughness is much weaker. Figures 11(c) and (f) plot the O_2 distribution 5 mm below the SWI for the two different burrow densities. For 4 ind./m^2, an ellipse-shaped area upstream of the mound receives injection of O_2 from the SWI at x=-10 cm to x=-5 cm. Downstream of the ellipse-shaped area, two regions with low O_2 concentration are found between the burrow inlet and outlet (x=-3.5 cm to x=0 cm) where convective flow is directed out of the bed. This behavior was also observed in the experiments by Huettel et al. (1996) and Ziebis et al. (1996b). For 120 ind./m^2, the distance between burrows are so small that the two enhanced O_2 injection areas in Figure 11(c) merge to form a large area with enhanced O_2 between burrows.

We also calculated the area-averaged effective diffusion coefficient *De/D'm* and compared it with the OH formula. Figure 12 shows that the OH formula underestimates the effective diffusion coefficient *De/D'm* by approximately a factor of 4 at 40 ind./m^2 and above. OH obtained their relationship using flume data over 2D sediment dunes and uniformly packed glass spheres. There is no significant transverse pressure difference in these flume experiments. However, in our simulation with 3D burrows, the transverse pressure difference also generated O_2 flux at SWI.

The effect of organism density and 3D flow is characterized by a dimensionless burrow number, Bu

$$\mathrm{Bu} = (\rho_{bio})^{1/2} k_s$$

where ρ_{bio} is the organism density in individuals/m^2 and k_s is the roughness height (m) for a single burrow. $(\rho_{bio})^{1/2}$ is the characteristic distance between burrows on the planar sediment surface. The two densities that do not deviate from the OH formula are for Bu<0.05 while the densities that conform to the fully 3D flow line have Bu of 0.13, 0.18 and 0.23 (18-120 burrow/m^2). 18 burrow/m^2 exhibits an effective transport rate intermediate between the two curves and has a Bu of 0.09. In general, it appears that Bu<0.05 suggests a flow that is effectively 2D while a Bu>>0.1 suggests a highly 3D flow and an oxygen transport approximately 4 times higher due to spanwise interactions. We further ran simulations of flow over 120 burrows/m^2 with different flow rates (2 cm/s to 16 cm/s) (also Figure 12). The oxygen transport at the high Bu (0.23) is consistent with $\frac{D_e/D_m'}{R_{e*}P_e^{1.2}} = a = 0.002$ over the entire range of $R_{e*}P_e^{1.2}$.

4 Discussion

An important question is the broader implications of this work for bioroughness and bioirrigation under other conditions or with different organisms. The model could be modified to address any burrow geometry and intensity and characteristics of bioirrigation, but the results suggest that at high roughness Reynolds number, the primary characteristic controlling transport of O_2 across the SWI is the roughness height. Thus, different organism burrow shapes and the extent of bioirrigation become less important to the O_2 transport. It is apparently for this reason that the relationship of OH is apparently applicable across a range of roughness types, heights and organisms at low organism densities. At high organism densities spanwise transport of O_2 increases the average O_2 rate but only by approximately a factor of 4 and the results appear independent of organism density after a transition from the approximately 2D flow over isolated roughness elements and organism burrows. In either case the effective O_2 transport rate scales well with $\mathrm{RePe_k}^{1.2}$ with only minor deviations over a range of permeability and O_2 degradation rates.

Deviations from the $\mathrm{RePe_k}^{1.2}$ scaling is only observed with bioirrigation and at low roughness Reynolds number. It is only in this range of low roughness Reynolds number that the effects of specific organism behavior including the nature and magnitude of bioirrigation are likely to become more important. Baranov et al. (2016b) show that with increasing burrow density, a density-dependent population feedback will arise and metabolic inhibition will lead to a decrease of the bioirrigation pumping activity. In our simulations, only observed field densities were used for simulations and the effects of density-dependent population feedback is not expected. Furthermore, D'Andrea and DeWitt (2009) show that the O_2 flux is linear with burrow density in steady water up to 600 ind./m^2 for *Upogebia pugettensis (Crustacea: Thalassinidae)*. Even at higher organism density that might lead to a decrease in bioirrigation, the roughness Reynolds number is also likely large and bioirrigation is not likely to significantly influence net O_2 transport and these conditions are unlikely to lead to deviations from $\mathrm{RePe_k}^{1.2}$ scaling.

While only U-shape burrows with mounds are investigated in our simulations, organisms also generate J-shape and Y-shape burrows and may not build mounds at the SWI (Kristensen et al., 2012). Mermillod-Blondin and Rosenberg (2006) show that in advection-dominated sediments, organism bioirrigation will not enhance O_2 consumption as significantly as organisms in gallery building. This phenomenon is further confirmed by Baranov (2018)

and Renz and Forster (2014). Mermillod-Blondin & Rosenberg (2006) suggested this was due to a reduction of availability of nutrients for bacteria and Renz & Forster (2014) suggested this was the result of different burrow depths and bioirrigation between organisms, but it appears from this work that the primary factor is turbulence generated by surface roughness. In our numerical simulations, we observed no influence of bioirrigation on the O_2 flux when $U_{water} \geq 8$ cm/s (Figure 9). The variations in burrow shape and organism behavior are likely to affect the internal distribution of O_2 even if it does not significantly change the overall O_2 transport. Understanding how the O_2 distribution changes would require simulations of the specific burrow geometry and organism types.

Although our focus was on net O_2 consumption due to bioroughness and bioirrigation, the O_2 transport and distribution can have other substantial effects. For example, bioirrigation has been observed to enhance heavy metal mobilization, such as Cd and Cu (He et al., 2017; Schaller, 2014), likely due to oxidation of reduced forms of Cd and Cu in the sediments (Hong et al., 2011a). The influence of hydrodynamics and bioirrigation on metal release can be further investigated by incorporating metal redox chemistry and transport into the current model. It may also be appropriate to extend the current work to unsteady mean overlying flow as our boundary conditions, e.g. due to cyclic changes in conditions such as pH or O_2 in the overlying water (Hong et al., 2011b) or consider dynamic biological processes such as intermittent bioirrigation (Volkenborn et al., 2012).

5 Conclusions

This study develops a model for O_2 transport from water to the sediment bed that integrates a LES description of the overlying water hydrodynamics with in-bed advective processes and organism-related bioroughness and bioirrigation. The main findings are as follows:

- Organism mounds and burrows substantially alter the surface roughness (bioroughness) and flow and oxygen transport over the SWI and the coupling between surface flow and subsurface flow.
- Bioirrigation also enhances oxygen transport and generates asymmetric distribution of O_2 around burrows although the influence of bioirrigation becomes negligible at high roughness Reynolds number
- The enhanced O_2 transport scales with roughness height and roughness Reynolds number- described well by OH ($D_e/D'_m = 0.005\, Re_*\, Pe^{1.2}$) when flow is effectively 2D, i.e. Bu = [burrow density]$^{1/2}$[burrow height]<0.05
- The O_2 transport increases by as much as a factor of 4 under mound-induced three-dimensional flow when there are substantial interactions between the flow over nearby mounds Bu>>0.1

Acknowledgments, Samples, and Data

This research is supported by the Donovan Maddox Distinguished Engineering Chair. The computations are supported by Texas Tech University's High Performance Computing Center (HPCC) using the in-house model code, Hydro3D. The simulation input files and model code are available at https://www.depts.ttu.edu/ceweb/groups/reiblesgroup/downloads.html.

References

Ahmerkamp, S., Winter, C., Krämer, K., Beer, D. d., Janssen, F., Friedrich, J., et al. (2017). Regulation of benthic oxygen fluxes in permeable sediments of the coastal ocean. *Limnology and Oceanography, 62*(5), 1935-1954.

Attard, K. M., Hancke, K., Sejr, M. K., & Glud, R. N. (2016). Benthic primary production and mineralization in a High Arctic Fjord: in situ assessments by aquatic eddy covariance. *Marine ecology progress series, 554*, 35-50.

Baranov, V. (2018). Influence of bioturbation on sediment respiration in advection and diffusion dominated systems.

Baranov, V., Lewandowski, J., & Krause, S. (2016a). Bioturbation enhances the aerobic respiration of lake sediments in warming lakes. *Biology letters, 12*(8), 20160448.

Baranov, V., Lewandowski, J., Romeijn, P., Singer, G., & Krause, S. (2016b). Effects of bioirrigation of non-biting midges (Diptera: Chironomidae) on lake sediment respiration. *Scientific reports, 6*, 27329.

Berg, P., Long, M. H., Huettel, M., Rheuban, J. E., McGlathery, K. J., Howarth, R. W., et al. (2013). Eddy correlation measurements of oxygen fluxes in permeable sediments exposed to varying current flow and light. *Limnology and Oceanography, 58*(4), 1329-1343.

Boudreau, B. (1997). A mathematical model for sediment-suspended particle exchange. *J. Mar. Syst, 11*, 279-303.

Boudreau, B. P., & Jorgensen, B. B. (2001). *The benthic boundary layer: Transport processes and biogeochemistry*: Oxford University Press.

Brand, A., Lewandowski, J., Hamann, E., & Nützmann, G. (2013). Advection around ventilated U‐shaped burrows: A model study. *Water Resources Research, 49*(5), 2907-2917.

Cardenas, M. B., & Wilson, J. L. (2007). Dunes, turbulent eddies, and interfacial exchange with permeable sediments. *Water Resources Research, 43*(8).

Cevheri, M., & Stoesser, T. (2018). Large-eddy simulation of a jet in crossflow using local mesh refinement. *Progress in Computational Fluid Dynamics, an International Journal, 18*(3), 137-149.

Cook, P. L., Wenzhöfer, F., Glud, R. N., Janssen, F., & Huettel, M. (2007). Benthic solute exchange and carbon mineralization in two shallow subtidal sandy sediments: Effect of advective pore‐water exchange. *Limnology and Oceanography, 52*(5), 1943-1963.

D'Andrea, A. F., & DeWitt, T. H. (2009). Geochemical ecosystem engineering by the mud shrimp Upogebia pugettensis (Crustacea: Thalassinidae) in Yaquina Bay, Oregon: Density‐dependent effects on organic matter remineralization and nutrient cycling. *Limnology and Oceanography, 54*(6), 1911-1932.

Elliott, A. H., & Brooks, N. H. (1997). Transfer of nonsorbing solutes to a streambed with bed forms: Theory. *Water Resources Research, 33*(1), 123-136.

Fang, H., Liu, Y., & Stoesser, T. (2017). Influence of Boulder Concentration on Turbulence and Sediment Transport in Open‐Channel Flow Over Submerged Boulders. *Journal of Geophysical Research: Earth Surface, 122*(12), 2392-2410.

Forster, S., Huettel, M., & Ziebis, W. (1996). Impact of boundary layer flow velocity on oxygen utilisation in coastal sediments. *Marine ecology progress series*, 173-185.

Frogner-Kockum, P., Göransson, P., Åslund, H., Ländell, M., Stevens, R., Tengberg, A., et al. (2016). Metal contaminant fluxes across the sediment water interface. *Marine pollution bulletin, 111*(1-2), 321-329.

He, Y., Men, B., Yang, X., Li, Y., Xu, H., & Wang, D. (2017). Investigation of heavy metals release from sediment with bioturbation/bioirrigation. *Chemosphere, 184*, 235-243.
Hölker, F., Vanni, M. J., Kuiper, J. J., Meile, C., Grossart, H.-P., Stief, P., et al. (2015). Tube‐dwelling invertebrates: tiny ecosystem engineers have large effects in lake ecosystems. *Ecological Monographs, 85*(3), 333-351.
Hong, Y. S., Kinney, K. A., & Reible, D. D. (2011a). Acid volatile sulfides oxidation and metals (Mn, Zn) release upon sediment resuspension: Laboratory experiment and model development. *Environmental Toxicology and Chemistry, 30*(3), 564-575.
Hong, Y. S., Kinney, K. A., & Reible, D. D. (2011b). Effects of cyclic changes in pH and salinity on metals release from sediments. *Environmental Toxicology and Chemistry, 30*(8), 1775-1784.Huettel, M., Berg, P., & Kostka, J. E. (2014). Benthic exchange and biogeochemical cycling in permeable sediments. *Ann Rev Mar Sci, 6*, 23-51. https://www.ncbi.nlm.nih.gov/pubmed/23987916
Huettel, M., & Gust, G. (1992). Impact of Bioroughness on Interfacial Solute Exchange in Permeable Sediments. *Marine ecology progress series, 89*(2-3), 253-267. <Go to ISI>://WOS:A1992KH34600014
Huettel, M., Ziebis, W., & Forster, S. (1996). Flow‐induced uptake of particulate matter in permeable sediments. *Limnology and Oceanography, 41*(2), 309-322.
Kelderman, P., & Osman, A. (2007). Effect of redox potential on heavy metal binding forms in polluted canal sediments in Delft (The Netherlands). *Water research, 41*(18), 4251-4261.
Koike, I., & Mukai, H. (1983). Oxygen and inorganic nitrogen contents and fluxes in burrows of the shrimps Callianassa japonica and Upogebia major. *Marine ecology progress series. Oldendorf, 12*(2), 185-190.
Kristensen, E., Penha-Lopes, G., Delefosse, M., Valdemarsen, T., Quintana, C. O., & Banta, G. T. (2012). What is bioturbation? The need for a precise definition for fauna in aquatic sciences. *Marine ecology progress series, 446*, 285-302.
Lai, J., Lo, S.-L., & Lin, C.-F. (1994). Effects of hydraulic and medium characteristics on solute transfer to surface runoff. *Water Science and Technology, 30*(7), 145-155.
Liu, Y., Stoesser, T., Fang, H., Papanicolaou, A., & Tsakiris, A. G. (2017). Turbulent flow over an array of boulders placed on a rough, permeable bed. *Computers & Fluids, 158*, 120-132.
Maerki, M., Wehrli, B., Dinkel, C., & Müller, B. (2004). The influence of tortuosity on molecular diffusion in freshwater sediments of high porosity1. *Geochimica et Cosmochimica Acta, 68*(7), 1519-1528.
McCall, P. L., & Tevesz, M. J. (1982). The effects of benthos on physical properties of freshwater sediments. In *Animal-sediment relations* (pp. 105-176): Springer.
Mermillod-Blondin, F., & Rosenberg, R. (2006). Ecosystem engineering: the impact of bioturbation on biogeochemical processes in marine and freshwater benthic habitats. *Aquatic Sciences, 68*(4), 434-442.
Murniati, E., Gross, D., Herlina, H., Hancke, K., & Lorke, A. (2017). Effects of bioirrigation on the spatial and temporal dynamics of oxygen above the sediment–water interface. *Freshwater Science, 36*(4), 784-795.
Murphy, E. A., & Reidenbach, M. A. (2016). Oxygen transport in periodically ventilated polychaete burrows. *Marine Biology, 163*(10), 208.
Nicoud, F., & Ducros, F. (1999). Subgrid-scale stress modelling based on the square of the velocity gradient tensor. *Flow, turbulence and Combustion, 62*(3), 183-200.
O'Connor, B. L., & Harvey, J. W. (2008). Scaling hyporheic exchange and its influence on biogeochemical reactions in aquatic ecosystems. *Water Resources Research, 44*(12). *Cited herein as OH*.

Ouro, P., Harrold, M., Stoesser, T., & Bromley, P. (2017). Hydrodynamic loadings on a horizontal axis tidal turbine prototype. *Journal of Fluids and Structures, 71*, 78-95.

Ouro, P., & Stoesser, T. (2017). An immersed boundary-based large-eddy simulation approach to predict the performance of vertical axis tidal turbines. *Computers & Fluids, 152*, 74-87.

Packman, A. I., Brooks, N. H., & Morgan, J. J. (2000). Kaolinite exchange between a stream and streambed: Laboratory experiments and validation of a colloid transport model. *Water Resources Research, 36*(8), 2363-2372.

Packman, A. I., Salehin, M., & Zaramella, M. (2004). Hyporheic exchange with gravel beds: basic hydrodynamic interactions and bedform-induced advective flows. *Journal of Hydraulic Engineering, 130*(7), 647-656.

Pascal, L., Maire, O., Volkenborn, N., Lecroart, P., Bichon, S., de Montaudouin, X., et al. (2016). Influence of the mud shrimp Upogebia pusilla (Decapoda: Gebiidea) on solute and porewater exchanges in an intertidal seagrass (Zostera noltei) meadow of Arcachon Bay: An experimental assessment. *Journal of Experimental Marine Biology and Ecology, 477*, 69-79.

Quintana, C. O., Hansen, T., Delefosse, M., Banta, G., & Kristensen, E. (2011). Burrow ventilation and associated porewater irrigation by the polychaete Marenzelleria viridis. *Journal of Experimental Marine Biology and Ecology, 397*(2), 179-187.

Reimers, C. E., Stecher III, H. A., Taghon, G. L., Fuller, C. M., Huettel, M., Rusch, A., et al. (2004). In situ measurements of advective solute transport in permeable shelf sands. *Continental Shelf Research, 24*(2), 183-201.

Renz, J. R., & Forster, S. (2013). Are similar worms different? A comparative tracer study on bioturbation in the three sibling species Marenzelleria arctia, M. viridis, and M. neglecta from the Baltic Sea. *Limnology and Oceanography, 58*(6), 2046-2058.

Renz, J. R., & Forster, S. (2014). Effects of bioirrigation by the three sibling species of Marenzelleria spp. on solute fluxes and porewater nutrient profiles. *Marine ecology progress series, 505*, 145-159.

Richardson, C., & Parr, A. (1988). Modified Fickian model for solute uptake by runoff. *Journal of environmental engineering, 114*(4), 792-809.

Santos, I. R., Eyre, B. D., & Huettel, M. (2012). The driving forces of porewater and groundwater flow in permeable coastal sediments: A review. *Estuarine, Coastal and Shelf Science, 98*, 1-15.

Savant, S. A., Reible, D. D., & Thibodeaux, L. J. (1987). Convective transport within stable river sediments. *Water Resources Research, 23*(9), 1763-1768.

Schaller, J. (2014). Bioturbation/bioirrigation by Chironomus plumosus as main factor controlling elemental remobilization from aquatic sediments? *Chemosphere, 107*, 336-343.

Teuchies, J., Bervoets, L., Cox, T. J., Meire, P., & De Deckere, E. (2011). The effect of waste water treatment on river metal concentrations: removal or enrichment? *Journal of soils and sediments, 11*(2), 364-372.

Uhlmann, M. (2005). An immersed boundary method with direct forcing for the simulation of particulate flows. *Journal of Computational Physics, 209*(2), 448-476.

Volkenborn, N., Hedtkamp, S., Van Beusekom, J., & Reise, K. (2007). Effects of bioturbation and bioirrigation by lugworms (Arenicola marina) on physical and chemical sediment properties and implications for intertidal habitat succession. *Estuarine, Coastal and Shelf Science, 74*(1-2), 331-343.

Volkenborn, N., Polerecky, L., Wethey, D., DeWitt, T., & Woodin, S. (2012). Hydraulic activities by ghost shrimp Neotrypaea californiensis induce oxic− anoxic oscillations in sediments. *Marine ecology progress series, 455*, 141-156.

Webb, A. P., & Eyre, B. D. (2004). Effect of natural populations of burrowing thalassinidean shrimp on sediment irrigation, benthic metabolism, nutrient fluxes and denitrification. *Marine ecology progress series, 268*, 205-220.

Xie, M., Wang, N., Gaillard, J.-F., & Packman, A. I. (2018). Interplay between flow and bioturbation enhances metal efflux from low-permeability sediments. *Journal of hazardous materials, 341*, 304-312.

Ziebis, W., Forster, S., Huettel, M., & Jørgensen, B. (1996a). Complex burrows of the mud shrimp Callianassa truncata and their geochemical impact in the sea bed. *Nature, 382*(6592), 619.

Ziebis, W., Huettel, M., & Forster, S. (1996b). Impact of biogenic sediment topography on oxygen fluxes in permeable seabeds. *Marine ecology progress series, 140*(1-3), 227-237. <Go to ISI>://WOS:A1996VJ37700021

Table 1. Hydrodynamics, mound morphology and burrow morphology of the numerical simulations.

Case	Hydrodynamics				Mound morphology		Burrow morphology		
	H_{water} [cm]	$H_{sediment}$ [cm]	U_{water} [cm/s]	U_{bio} [cm/s]	Height [cm]	Width [cm]	Depth [cm]	Length [cm]	Diameter [cm]
Flat	5	10	2~16	-	-		-		
Bioroughness	5	10	2~16	-	1	4	5	10	2
Bioirrigation	5	10	2~16	2	1	4	5	10	2

Table 2. Comparison of the hydraulic parameters used in our Bioroughness simulations with experimental data.

Source	D_{50} [mm]	k [10^{-6} m^2]	ø	k_s [cm]	L [cm]	u_* [cm/s]	U [cm/s]	H [cm]
Richardson	0.1~3.0	0.17~71	0.36~0.40	-	-	0.3~1.3	3.7~22.9	0.6~1.9
Lai	0.5~3.2	2.3~19	0.36~0.38	-	-	0.2~0.6	7.4~15.4	0.5~2
Elliott	0.1~0.5	0.08~1.1	0.30~0.33	1.1~2.5	9~30	1.3~2.4	8.6~13.2	3.1~6.5
Packman	0.5	0.58~1.8	0.29~0.38	0~3.7	0~32	1.1~3.2	9.0~36.1	11.3~20.5
Current Study	0.35	0.51	0.40	1.0	30-75	0.22~1.72	2.0~16.0	5.0

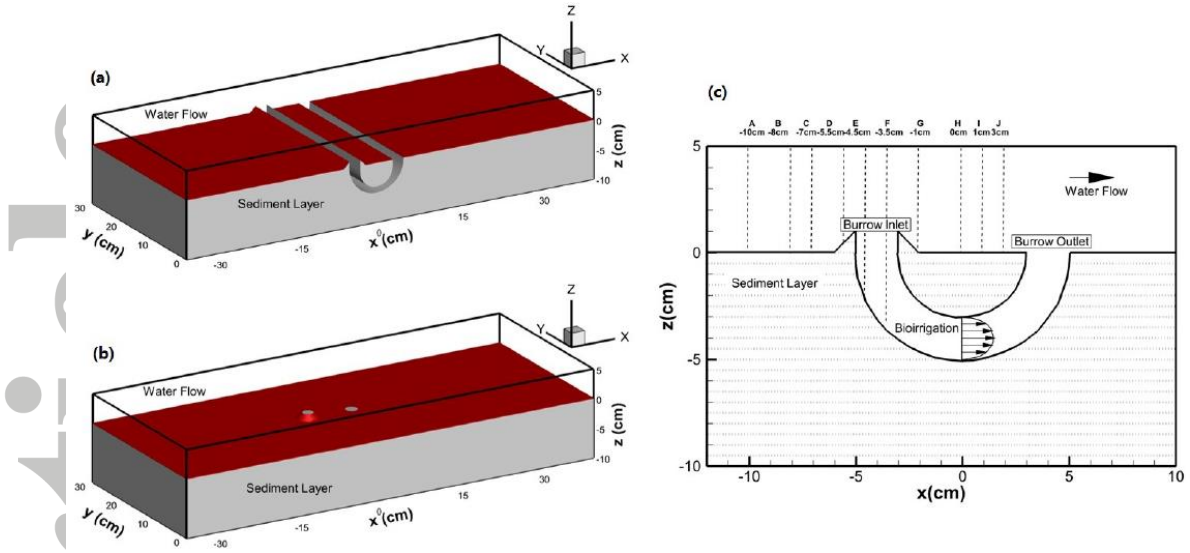

Figure 1. Numerical setup of the computational domain. a) flow over a 2D burrow; b) flow over a 3D burrow; c) longitudinal section (XZ) of the burrow.

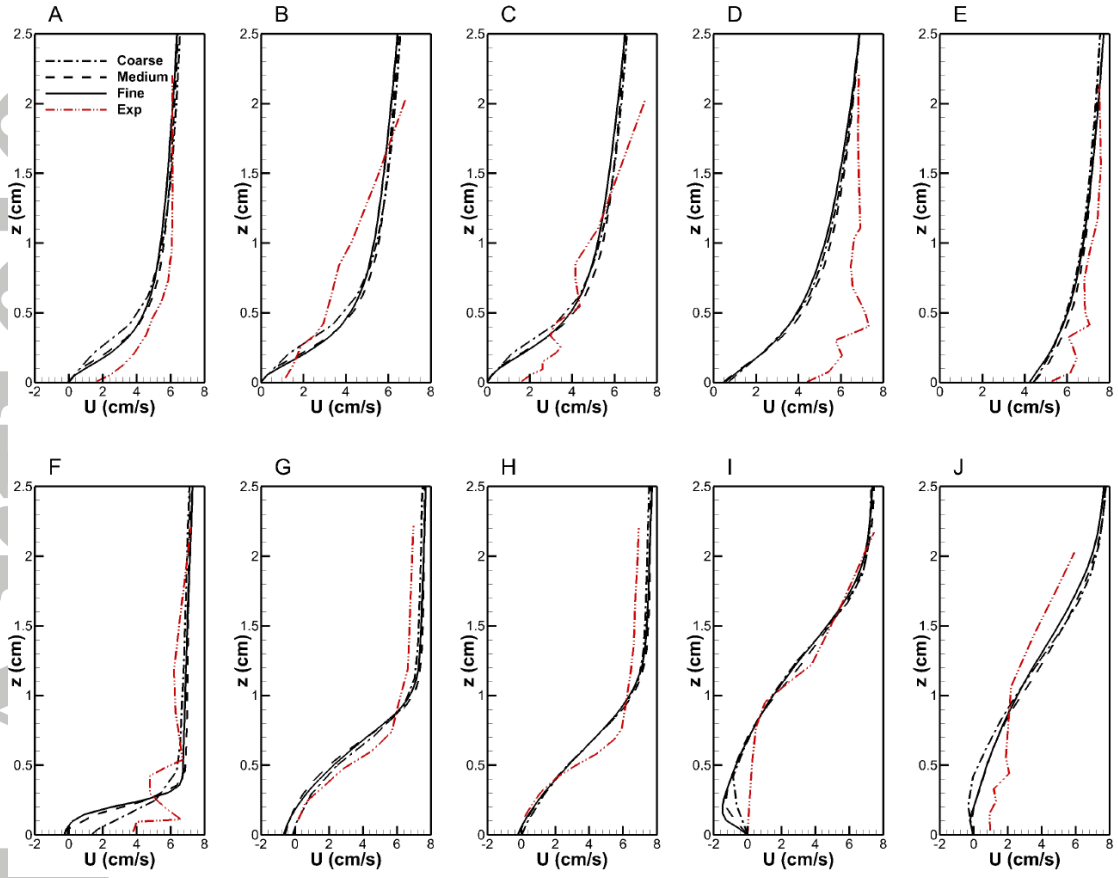

Figure 2. Time-averaged streamwise velocity profiles at cross sections A to J for three different meshes.

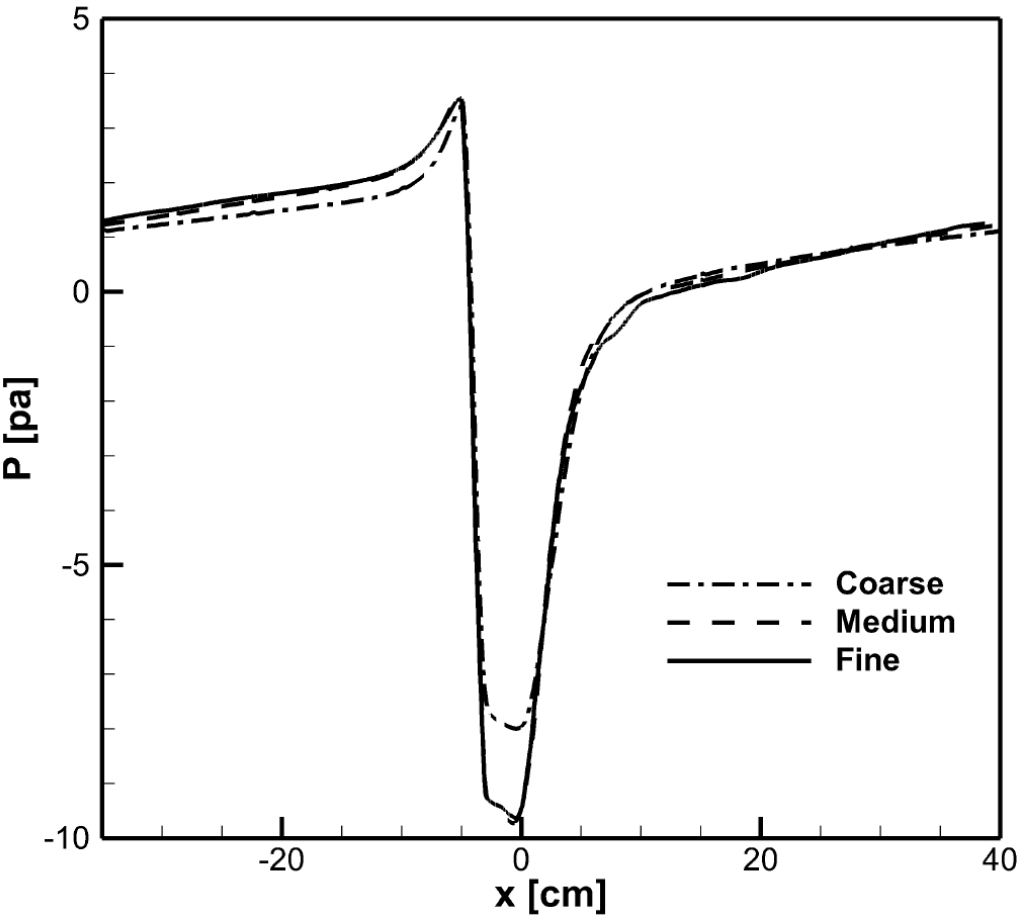

Figure 3. Time-averaged pressure distribution along the SWI for three different meshes.

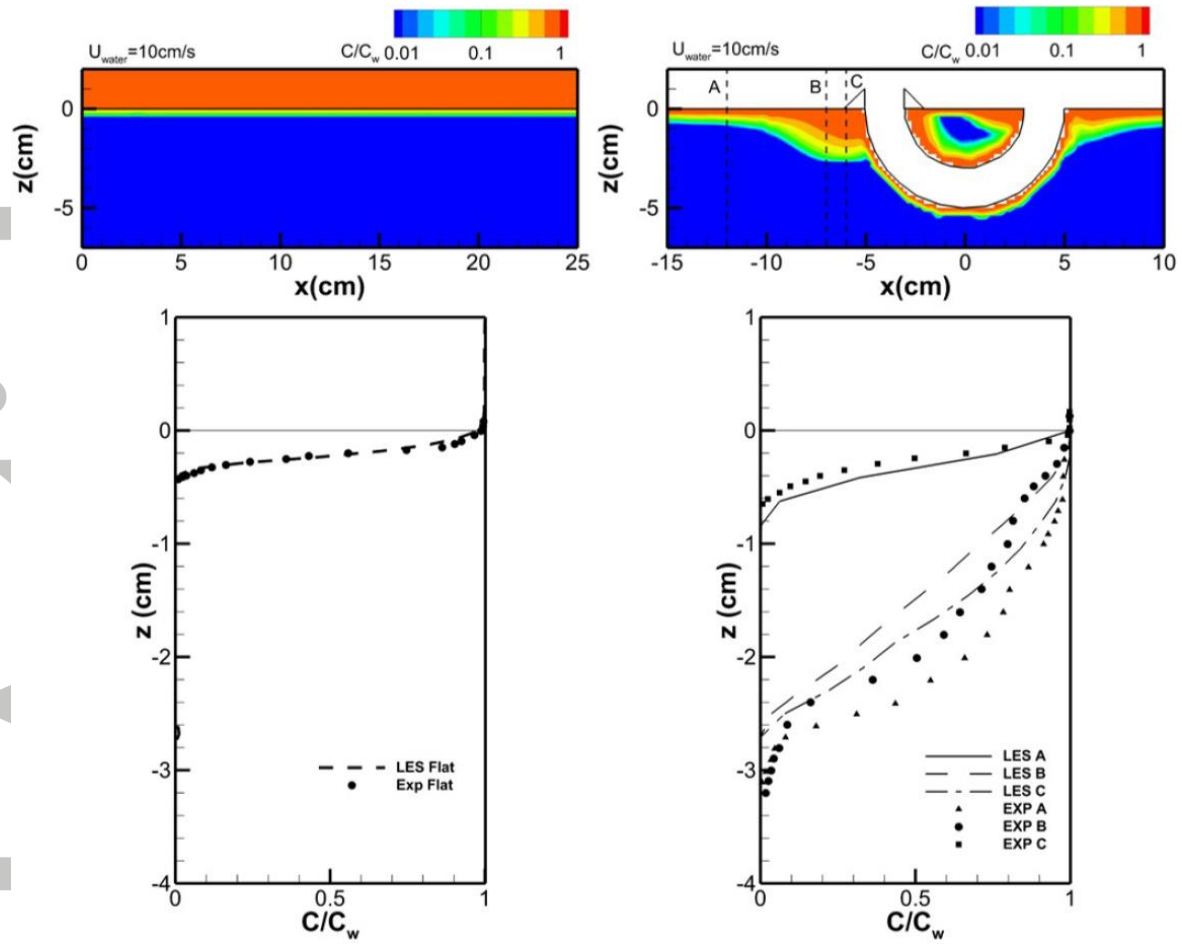

Figure 4. Time-averaged O_2 distribution and O_2 profiles for flow over flat sand bed (left column – no burrows or mounds) and bed with bioroughness (right column).

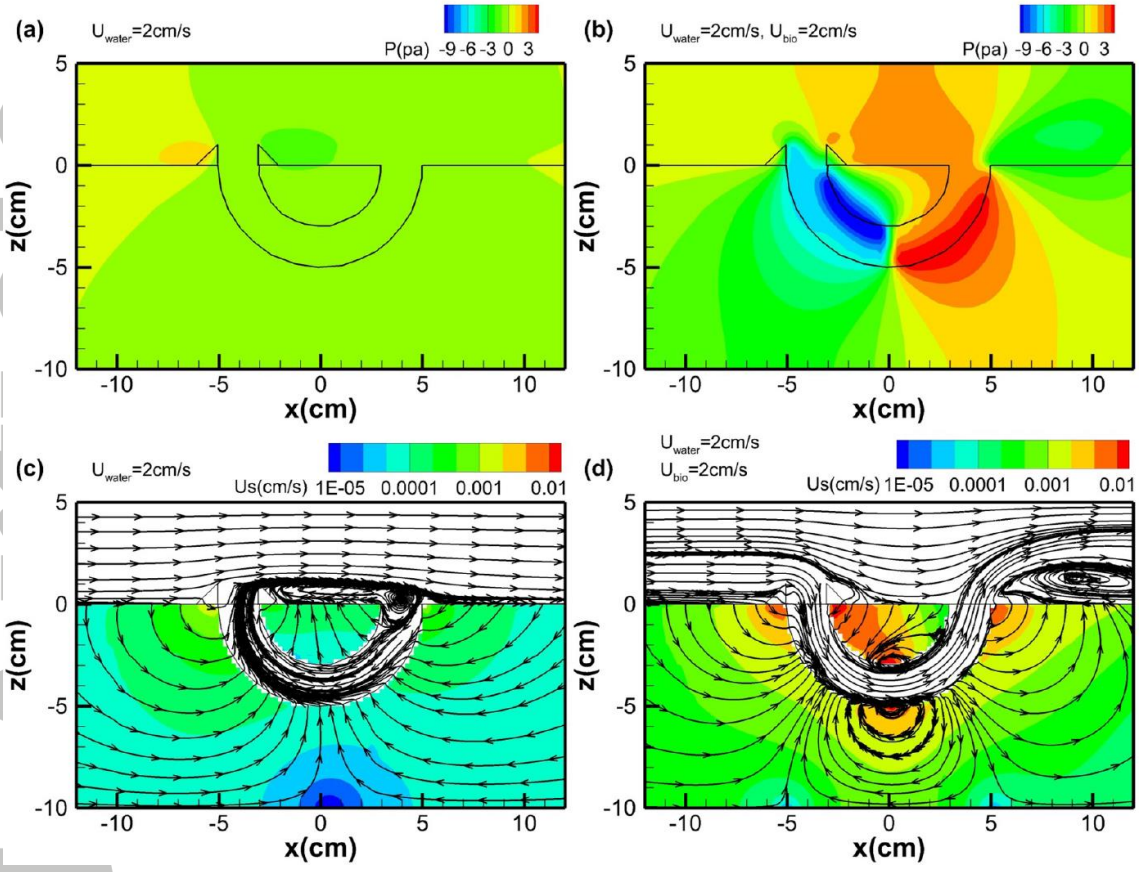

Figure 5. Time-averaged pressure and velocity contours with streamlines for simulations U_{water}=2 cm/s without (left column) and with bioirrigation (right column).

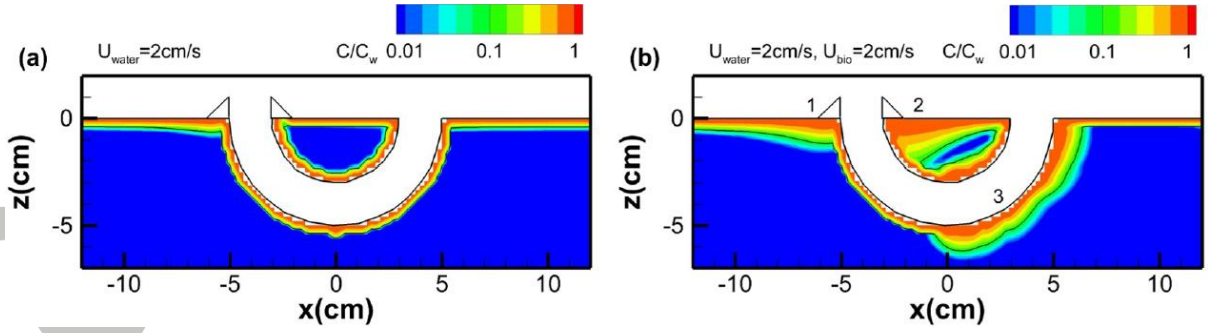

Figure 6. Time-averaged O_2 concentration in the sediment for case Bioroughness (left column) and Bioirrigation (right column) with U_{water}=2 cm/s.

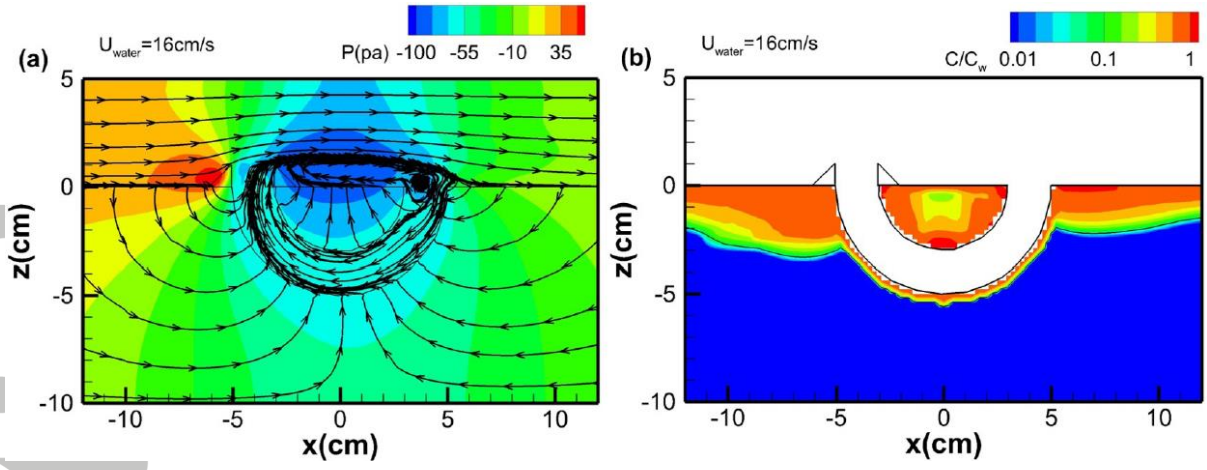

Figure 7. Time-averaged pressure distribution and O_2 concentration for bioroughness case with U_{water}=16 cm/s.

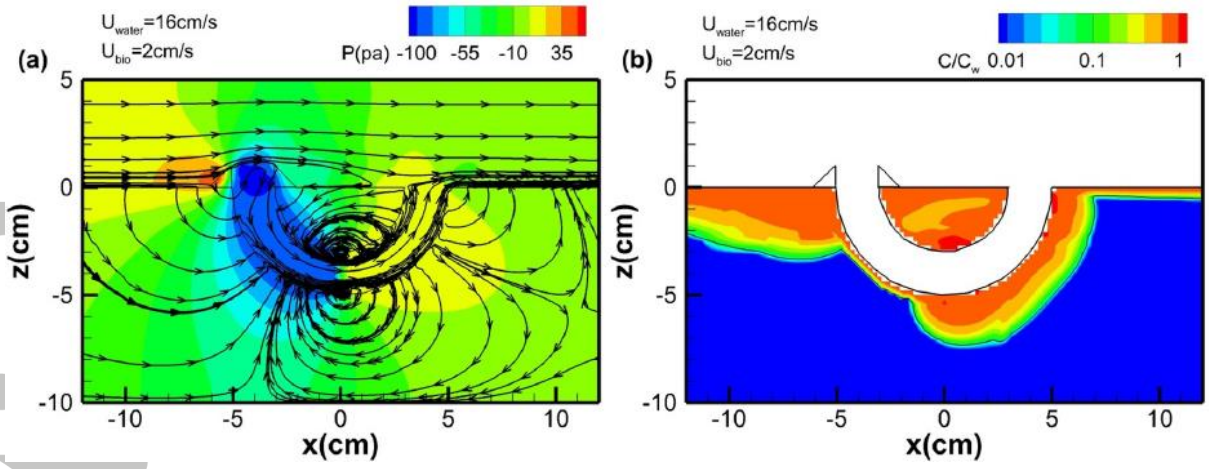

Figure 8. Time-averaged pressure distribution and O2 concentration for case bioirrigation with U_{water}= 16 cm/s.

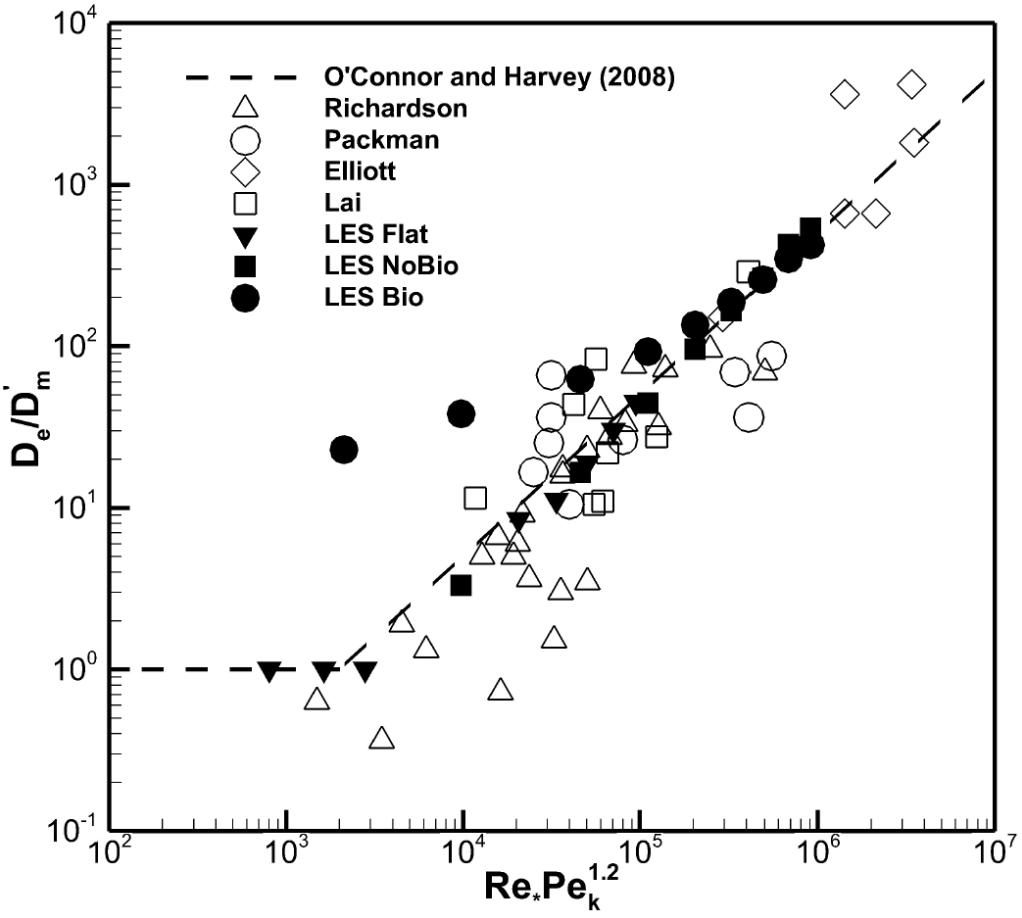

Figure 9. Dimensionless effective diffusion coefficient, *De/D'm*, calculated from our LES simulations and from several flume experiments along with the empirical formula proposed by OH.

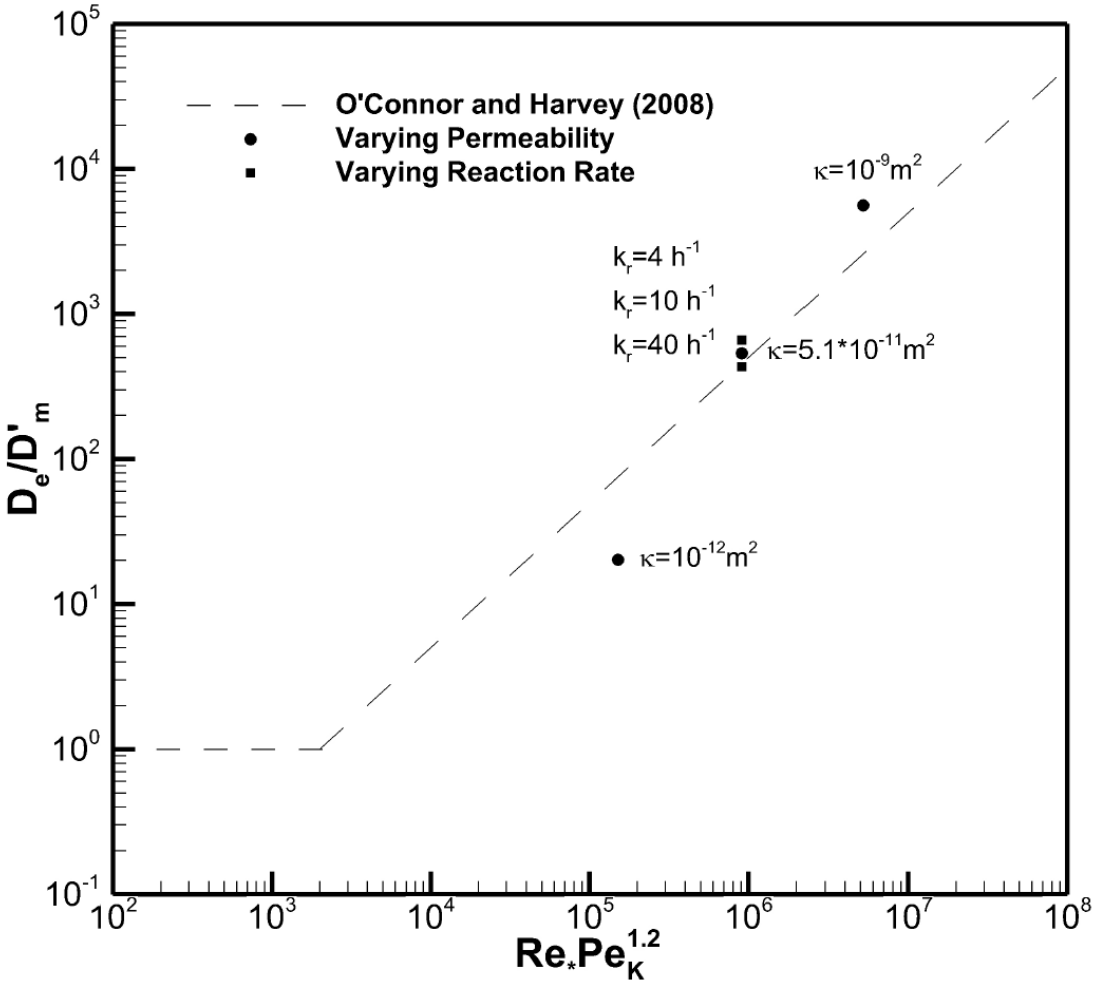

Figure 10. Influence of changes in O_2 reaction rate constant and bed permeability on net O_2 transfer rate

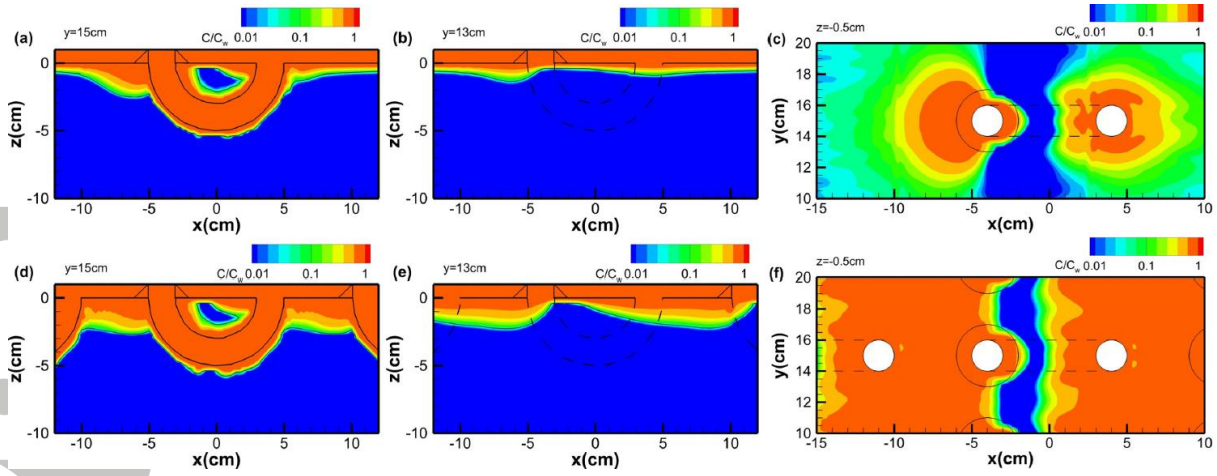

Figure 11. O_2 distribution around a 3D burrow with density 4 ind./m^2 (top) and 120 ind./m^2 (bottom) along the burrow centerline (a and c), 1 cm outside of the burrow in the spanwise direction (b and e) and in the horizontal plane 0.5 cm into the sediment (c and f).

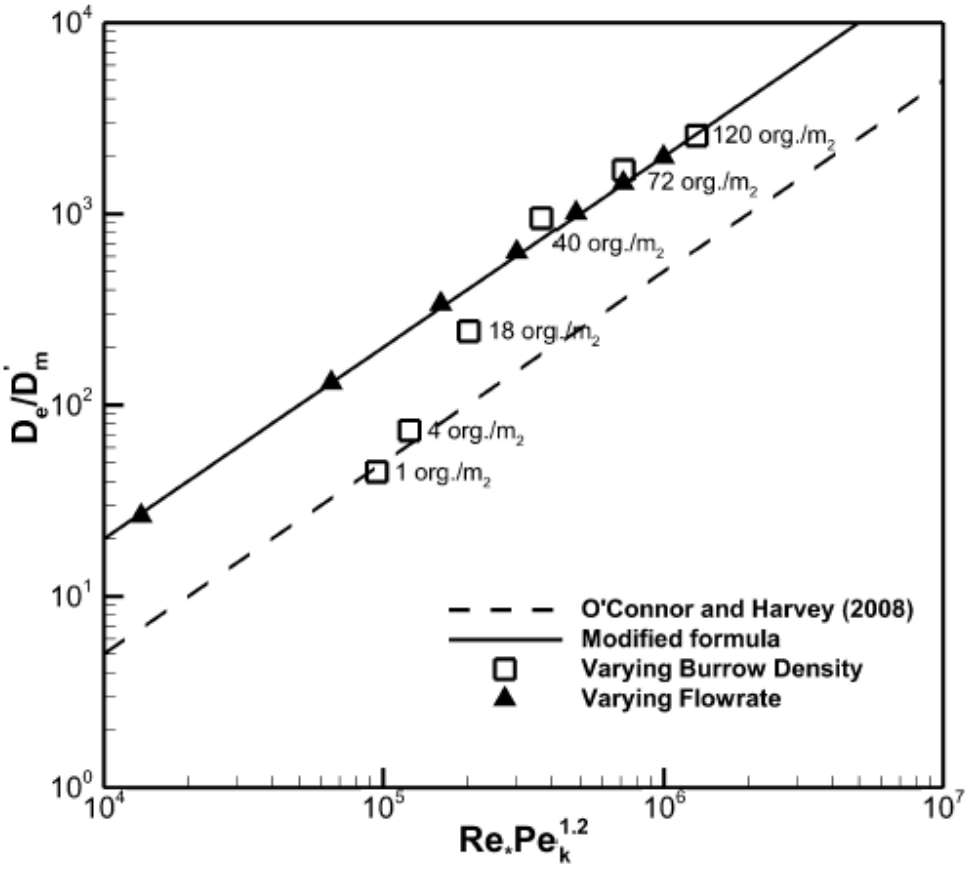

Figure 12. The dimensionless effective diffusion coefficient, *De/D'm* for simulations with different burrow individual densities (open squares) and different flow rates (solid triangle) with the OH empirical formula (broken line). Solid line is $0.002\ Re_*\ P\ e^{1.2}$ for 3D simulation of high burrow density